Absolute extreme ultraviolet yield from femtosecond-laser-excited Xe clusters

S. Ter-Avetisyan,[1,2] M. Schnürer,[1] H. Stiel,[1] U. Vogt,[1] W. Radloff,[1] W. Karpov,[1,3] W. Sandner,[1] and P. V. Nickles[1]
[1]*Max-Born-Institut, Max-Born-Straße 2a, D-12489 Berlin, Germany*
[2]*Institute for Physical Research, Ashtarak-2, 378410, Armenia*
[3]*General Physics Institute, Moscow, 117942, Russia*

(Received 18 December 2000; revised manuscript received 26 April 2001; published 28 August 2001)

Large Xe clusters (10^5-10^6 atoms per cluster) have been irradiated with ultrashort (50 fs) and high-intensity ($\sim 2\times 10^{18}$ W/cm^2) pulses from a Ti:sapphire multi-TW laser at 800 nm wavelength. Scaling and absolute yield measurements of extreme ultraviolet (EUV) emission in a wavelength range between 7 and 15 nm in combination with cluster target characterization have been used for yield optimization. Maximum emission as a function of the backing pressure and a spatial emission anisotropy covering a factor of two at optimized yields is discussed with a simple model of the source geometry and EUV-radiation absorption. Circularly polarized laser light instead of linear polarization results in a factor of 2.5 higher emission in the 11 to 15 nm wavelength range. This indicates the initial influence of optical-field ionization for the interaction parameter range used and contrasts to collisional heating that seems to influence preferentially higher ionization. Absolute emission efficiency at 13.4 nm of up to 0.5% in 2π sr and 2.2% bandwidth has been obtained.

DOI: 10.1103/PhysRevE.64.036404 PACS number(s): 52.50.Jm, 36.40.Vz

I. INTRODUCTION

The interaction of high-intensive laser radiation with ''van der Waals'' clusters has received increased attention in the recent past, especially because they may be capable of producing sufficient flux in the EUV region for key technologies and intriguing applications, such as extreme ultraviolet (EUV) lithography, spectroscopy, and microscopy [1–3]. Due to the near solid density of a single cluster object that consists of several hundred, up to millions of atoms, in a nanometer-sized volume and a gaseous average atomic density of a cluster ensemble within the extension of a micrometer-sized laser focus, an attractive combination of different properties results. Because the disassemble time of laser heated ''van der Waals'' clusters is on a picosecond time scale, an effective high-intensity laser interaction is anticipated during pulse widths similar or shorter as this characteristic time scale. Meeting this condition, high-laser absorption efficiency could be demonstrated [4], which leads to large energy deposition in the target. Therefore, a lot of work was devoted to study laser-cluster interaction phenomena, which give significant emission of short wavelength light in the spectral range of the EUV region [5] up to hard x rays [6]. Moreover, energetic ions from exploding clusters [7,8] have been analyzed and attributed to different excitation mechanisms [5,9].

Furthermore, laser-driven cluster targets are debris free, which is a significant problem for solid-state targets providing efficient emission in the whole EUV and x-ray range as a predominant feature. This constraint is more severe if only a high-pulse repetition rate can provide a sufficient photon flux for the applications. Thus, atomic clusters from heavy rare gases are interesting candidates to meet a required high EUV and x-ray brightness from a debris-free source. The advances in ultrafast laser technology are paving the way to compact high-repetition and high-intensity drivers for short wavelengths laboratory sources, which has to include ongoing research on suitable target systems.

In this paper, we direct our view to the spectral region between 7 and 15 nm emitted by Xe clusters that is currently under intensive investigation as a highly attractive wavelength region for future lithographic systems [10–12], serving as a key technology for the fabrication of microchips with structure sizes smaller than 0.1 μm [13].

We have used a 50 fs multi-TW Ti:sapphire system as a driver for ultrafast laser excitation of Xe clusters. Photon yields have been measured in absolute terms in a range between 10 and 15 nm that provides the basis for comparison to other experiments where different laser parameters, e.g., the wavelength (248 nm [14]) were used. First, we describe our experimental setup and measurements for cluster size. Varying these measures, we have optimized the photon yield in different spectral regions that was to our knowledge not done so far. In the following, we discuss the results in context to cluster excitation or heating models. Furthermore, we include data obtained with different laser polarization in the process of EUV-yield optimization.

II. EXPERIMENTAL SETUP

The experimental setup in the target chamber is shown in Fig. 1. The experiments have been carried out with 50 fs laser pulses at 800 nm center wavelength from a 10 Hz repetition rate multi-TW Ti:sapphire laser [15] at Max-Born-Institute. We used a 4 TW (200 mJ) beam of 60 mm in diameter, which was delivered via evacuated tubes from the vacuum compressor chamber to the interaction chamber. The beam is focused with an $f/2$ off-axis parabolic mirror having a focal length of 155 mm. The focus size was determined by imaging the attenuated beam onto a normal video 8-bit charge-coupled device (CCD)-camera. With a beam waist $w_0=5$ μm and the estimated energy content in a spot of a $d=2w_0$ diameter an interaction intensity of $\sim 2\times 10^{18}$ W/cm^2 was inferred. This intensity level was verified under comparable conditions in single-atom ionization experiments [16].

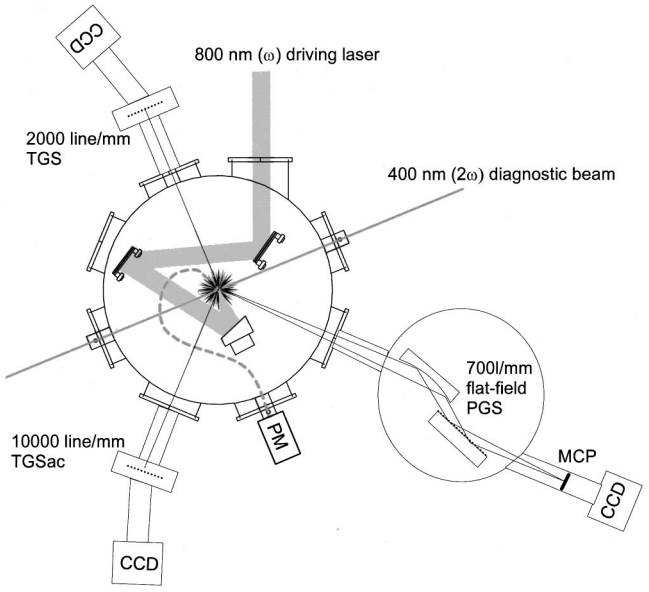

FIG. 1. Experimental setup at the vacuum interaction chamber including the Xe-cluster jet target: PM, photomultiplier coupled to an optical fiber for scattered light detection using the 400 nm diagnostic beam; TGS, transmission grating spectrograph (on axis, which refers to the incident laser beam axis); TGSac, absolute calibrated transmission grating spectrograph (off axis); PGS, plane (flat field) grating spectrograph with MCP, microchannel plate detector.

The Xe-cluster target was formed by expanding the gas from pressures up to 55 bar and a temperature of $T_0 = 300\,\mathrm{K}$ through the hypersonic conical nozzle with a cone angle $2\theta = 7°$, throat diameter of 400 μm, and an 8 mm-long conical section. For target optimization and system synchronization, the cluster beam is pulsed by an electromagnetic valve for every 3 sec with a pulse duration of 5 ms, which keeps the background pressure before each gas pulse on a 10^{-6} mbar level. The laser focus is placed approximately 1 mm below the orifice of the nozzle and the laser-beam axis crosses the cluster beam at a right angle.

Soft x-ray spectra were measured with two transmission spectrometers and one flat-field grazing incidence spectrometer allowing us the simultaneous registration of x-ray emission at different angles relative to the incident laser-beam axis. One transmission grating spectrometer (TGS, on-axis) is looking at the target along the laser beam in axial direction (grating 2000 lines/mm, resolution $\lambda/\Delta\lambda = 60$ at 13 nm) covering the spectral region 5–20 nm. At 45° to the laser-beam axis, a second transmission grating spectrometer) is installed (grating 10 000 l/mm, resolution $\lambda/\Delta\lambda = 300$ at 13 nm, comparable to those described in [17]), which is absolute calibrated (TGSac, off axis) in the wavelength range between 10 and 15 nm at the synchrotron facility BESSY II (Physikalisch Technische Bundesanstalt beamline). In both cases, the spectra are registered with back-illuminated thinned 512×512-pixel CCD x-ray cameras (photometrics, scientific instruments). Optical light is blocked with 200 nm Zr filters. We integrated the spectra over nine laser shots for quantitative analysis although it was also possible to monitor the x-ray emission on each shot. A third flat-field grazing incidence EUV spectrograph with a varied spacing grating (average spacing 700 l/mm, resolution $\lambda/\Delta\lambda = 300$ at 13 nm) was used at the same angle as the TGSac acting in a single-shot mode for qualitative comparison of the EUV emission within target and laser-beam alignment. Here, the detection system is realized with a multichannel plate-phosphorous screen combination, which is read out with an optical sensitive CCD camera.

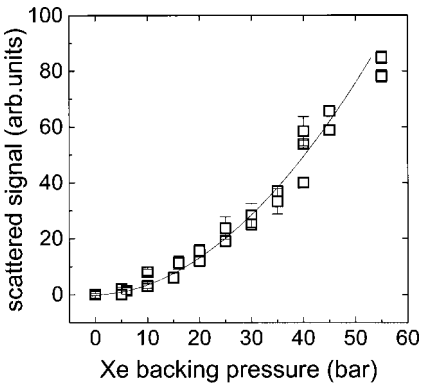

FIG. 2. Rayleigh scattered signals (S) from growing Xe clusters in dependence from the backing pressure (p), fit curve is $S \propto p^{1.9}$.

III. CLUSTER SIZE CHARACTERIZATION

The clusters in the beam were formed by supersonic gas expansion through a pulsed conical nozzle into a vacuum that can be characterized by the condensation scaling parameter Γ^* of Hagena and Obert [18,19]. It was shown that with $\Gamma^* > 5\times10^4$, one can expect large cluster formation ($>10^4$ atoms/cluster). With our geometry (jet throat diameter 400 μm, jet expansion half angle $\theta = 3.5°$) and an initial gas temperature of $T = 300\,\mathrm{K}$ for Xe already at 5 bar a parameter $\Gamma^* \geqslant 10^5$ results (see, e.g., [20]). Employing Hagena's formula from [19] and the concept of equivalent nozzles, a value of $\approx 2\times10^6$ atoms/cluster at 5 bar is derived.

Because the actual values may be influenced by further specifics [19] that are not included in Hagena's formulas, the presence of clusters in the gas jet was analyzed with a Rayleigh scattering technique [21]. The Rayleigh scattering cross section is proportional to λ^4 and thus the cluster gas jet was probed by a doubled-laser frequency $2\omega_0(400\,\mathrm{nm})$ beam having a pulse energy of 100 μJ and a pulse width of 200 ps. The beam diameter was 1.5 mm. In order to reduce the background of unwanted scattered light, the entrance and the exit windows of the chamber, which are passed by the diagnostic beam, are mounted with two additional tubes at a distance of 2 m from the gas jet. Scattered light from the clusters was collected with a 2.5 mm diameter aperture of a glass fiber cable looking at 90° with respect to the diagnostic beam axis. The scattered photons were registered with a photomultiplier tube (Hamamatsu R928) and additionally for some backing pressures in absolute terms using a cooled CCD camera with known quantum efficiency. In order to exclude shot-to-shot laser energy fluctuation the (scattered light)/(incident laser light) relation was measured. Figure 2 shows the scattered

light signal as a function of backing pressure. Scattered signals above the noise level were observed starting from 5 bar and increasing nonlinearly with backing pressure. In some work where nozzles with large expansion angles have been applied, the observed scattered signals S scaled with backing pressure p_0 as $S \propto p_0^3$ [22]. Our measurements between 5 and 55 bar indicate that the scattered signal scales with backing pressure as $\sim p_0^{1.9}$ that gives an exponent somewhat lower than in [23]. This deviation prompted us to compare predicted values by Hagena's formula with an absolute cluster size determination.

In general, one meets several difficulties in order to access all parameters that determine the absolute size of the scattering signal (see, e.g., Bell *et al.* [24] and [25,26]). We determined at some backing pressures, scattered photon numbers in absolute terms. The decrease of the average density in a nozzle flow [19] was used, which gives the number of atoms in the scattering volume if its appropriate size is taken. Therefore, our estimations are subjected to relatively large uncertainties. A quantitative estimation of the cluster size based on scattered photon numbers and assuming 100% condensation into clusters gives about $(2-6)\times 10^6$ atoms/cluster at 20 bar backing pressure. With a linear relation between cluster number and backing pressure [5], we calculate on the basis of our measured dependence of the scattered signal $S \propto p_0^{1.9}$ cluster sizes of $(3-10)\times 10^5$ atoms at 5 bar and of $(2-8)\times 10^6$ atoms at 50 bar.

An optical thick target is one prerequisite for good laser light absorption and efficient ionization for short wavelengths emission of desired ionic species. The absorption behavior was determined by a measurement of the laser energy transmitted through the target as a function of the backing pressure. However, this method implies a low level of scattering and reflection of the high-intensity laser beam. Several works [4,14,27–29] have relied on this. Zweiback, Ditmire, and Perry [29] measured for targets containing large clusters (up to 6×10^5 atoms/cluster) that the scattered intensity in different directions, as well as forward and backscatter, is negligible and below 1% of the total incident light. Therefore, the transmitted energy of the driving laser through the cluster target can be related to the absorption characteristic. In the case of our measurement, we also make use of the detector of the on-axis spectrograph. Because the entrance pinhole (50 μm diameter) of the spectrograph is aligned along the laser beam axis, some laser light penetrating through the 200 nm Zr filter (few percent transmission at 800 nm) and diffracted by the pinhole can be detected on the CCD in the surrounding of the zero order of the grating spectrometer. This illuminated area is clearly distinguishable from the EUV-spectral traces and can be used to derive a signal that scales linearly with the laser light signal, having passed the target and impinges to the entrance of the spectrograph. The laser light transmission curve in Fig. 3, obtained in such a way, shows that the cluster target can really form a dense object for powerful optical femtosecond laser pulses [4,26] and already at low pressures, a sharp decrease in the transmission is evident. The drop in transmission, as discussed above, is mainly due to enhanced laser light absorption because back and side scattering seems not to be predominant [29]. The obtained characteristics will be related to the EUV-emission results that are discussed in the next paragraph. The visible small maximum between 10 and 25 bar in the transmission curve was reproducible and probably not a bare valve characteristic. Its origin was not investigated further because no special x-ray signal variation has been found in relation to it.

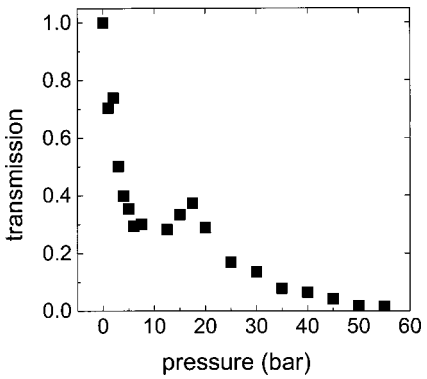

FIG. 3. Measured transmission of the 50 fs, 800 nm Ti:sapphire laser, focused at $\sim 2\times 10^{18}$ W/cm^2 in to the Xe-cluster target in dependence from Xe backing pressure.

IV. EUV YIELD IN DEPENDENCE FROM TARGET CHARACTERISTICS

In Fig. 4, we depict spectra from the on-axis spectrometer obtained with different backing pressures. Three broadband emission peaks were observed in the 1 to 16 nm wavelengths range. The emission between 10.5 and 16 nm is well known from literature [30–32]. Four emission peaks were observed in this region that come from Xe^{9+} to Xe^{11+} ions. Most of the intensive EUV emission occurs at certain xenon ion stages and relates generally to transitions from resonance levels to the ground state of the respective ion. The emission region from 6 to 9 nm (138 to 206 eV) has been observed in

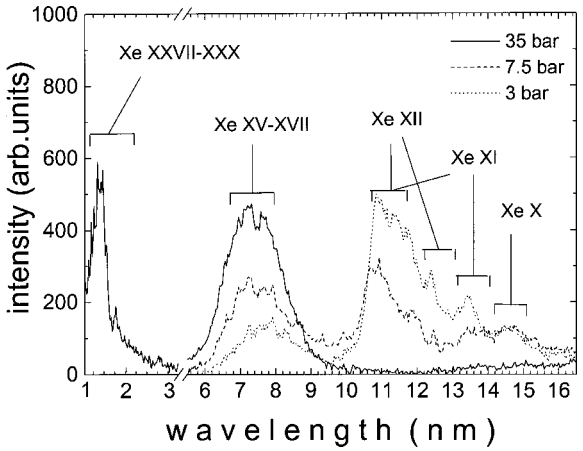

FIG. 4. Spectra at 3, 7.5, and 35 bar Xe backing pressure registered with the on-axis TGS and marks of emission line bands from different Xe ion stages. Emission between 1 and 2 nm is not shown for low-pressure values because of an apparent optical background signal (see Fig. 3 and explanation in the text).

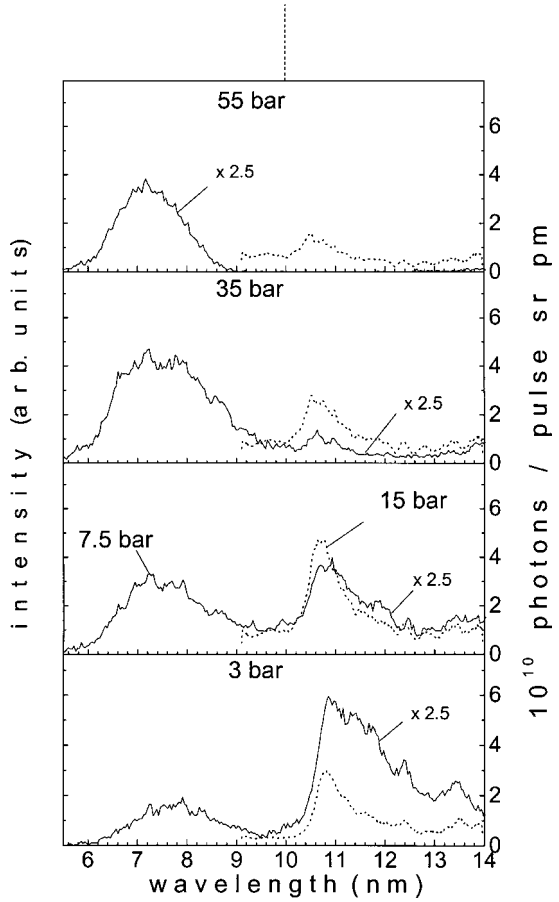

FIG. 5. On-axis (solid line) and off-axis (dotted line) spectra with absolute photon numbers (right axis) for wavelengths above 10 nm at relevant Xe backing pressures. (On-axis spectra have been scaled down for better comparison.) Values below 10 nm (dashed division line) refer to the relative intensity scale (left axis).

some spectral measurements [33,34], but it was not addressed in further discussions. Taking into account that a typical relation between the energy of main contributing resonance states and the ionization energy is ~1/2 [35], Xe (XV–XVII) and higher ion stages can have strong contributions in this emission region. Between 6 and 7 nm the recorded signal decreases due to the transmission characteristic of the Zr filter. Strong emission in the 1 to 2 nm wavelengths region (Xe XXVII–Xe XXX) [36,37] was also observed (see Fig. 4) but not investigated further in this paper.

A strong influence of the backing pressure and related target characteristics on the shape of the spectrum is already visible in Fig. 4. We investigated this behavior in more detail and put a typical collection of spectra into Fig. 5. The full line represents the signal from the on-axis TGS (6–14 nm) and the dotted one from the 45° off-axis TGSac (10–14 nm) which is absolutely calibrated in this range. With the help of a special cross-calibration experiment, where both spectrometers looked at the same angle to the radiating plasma object, we can infer absolute photon numbers also from the second TGS. The signals below 10 nm refer to a relative scale in Fig. 5.

Starting from 1 bar, we found an optimum pressure for maximized emission around 11 and 13 nm. The maximum yield in on-axis emission was registered at 3 bar and that in 45° off-axis direction at 15 bar backing pressure. A further pressure increase leads to a continuous drop of the 11 to 13 nm emission band up to a vanishing signal in on-axis direction, while in off-axis direction, this spectral signal keeps visible at a 3–4 times reduced level. On the other hand we observed a continuous increase of the 6–9 nm band with increasing pressure up to 35 bar and a slightly following decrease up to 55 bar pressure. This part of spectra was only measured with the lower dispersive TGS in the on-axis direction because we paid more comparative attention to the 13 nm region in this series of experiments.

For intense laser-pulse interaction with gaseous targets containing large atomic clusters, a formation of high-density plasma ''balls'' is anticipated, which leads to an efficient laser energy absorption (cf. Fig. 3). Furthermore, in analogy to plasmas produced from solid-state targets, high-ionization states can be produced via collisions before expansion disassembles the small plasma cluster ball. After expansion, the properties of our plasma will be similar to a low-density plasma. In the case of our relevant cluster sizes, hydrodynamic expansion is predominant and the cluster expansion time τ_{ex} is approximately [5]

$$\tau_{\mathrm{ex}} \approx r_c [m_i/(ZkT_e)]^{1/2} (n_c/n_s)^{1/3}, \tag{1}$$

where r_c, n_c is the initial cluster radius and density, respectively, n_s is the surrounding average gas density, kT_e is the cluster electron temperature, and Z is the average charge per ion with a mass m_i in the cluster. In the case of a Xe cluster with a 40 nm diameter ($\sim 10^6$ atoms/cluster) and heated to an initial electron temperature of $kT_e = 1000\,\mathrm{eV}$ [38], one obtains an expansion time of ~6 ps. In general, one can conclude that increased cluster size increases the laser light absorption because the ions in the cluster hold together for a longer time and favoring, thus, the energy-transfer processes that act efficiently at high electron and ion densities. At already low pressures with the onset of cluster formation, a sharp decrease in the transmission of the heating laser beam through the cluster target occurs as visible in Fig. 3. This fits well with growing cluster size as it is manifested in Fig. 2 from the Rayleigh scattering experiments.

The collection of our spectra in Fig. 5 shows the emission characteristics of our target as a function of the backing pressure. Qualitative changes in the spectra are observed with both our spectrometers, the on-axis and off-axis one. But the pressure ranges where maximum and minimum emission occur are different. In the case of the on-axis spectrometer, the emission signal between 11 and 13 nm is very low at pressures above 30 bar. In contrast to lower pressures, the maximum on-axis signal is 2–3 times higher compared to the maximum signal from the off-axis spectrometer. Although we cannot give a detailed solution on this question, we want to make some arguments and simple calculations that could count for this differing behavior.

Our gas-cluster target has an extension of approximately 1.4 mm (orifice diameter). Inside we produce the heated plasma emission source. If we relay the focusing conditions

(confocal length $2\pi w_0^2/\lambda$, diameter $2w_0$) to the extensions of the produced plasma object, the spectrometers look to an object, which has probably a much shorter (10–20 times) transverse dimension compared to its main axis (≡laser axis) (similar to source pictures in [14]). Because the observation solid angles of the spectrometers are large enough, one would not expect different signals due to the detection geometry.

Registered signals may be influenced if absorption comes significantly into play. Based on Hagena's scaling laws [18,19] we estimate a concentration drop of Xe to a 1% level in the target region compared to the stagnation chamber. Thus, high backing pressures (50 bar) give average atom densities of xenon, which relate to already short absorption length. At 50 bar and photon energies of 95 to 115 eV (10.8 to 13 nm) the absorption length amounts to 30–40 μm, at 177 eV (7 nm) the absorption length is 800 μm [39].

Different registered signals may result if the radiation passes different lengths of the absorbing medium. In our target, such a situation may occur if the radiation emitting plasma object is not placed in the center of the ambient cluster gas. Miura, *et al.* [14] showed with a series of source images how an ultrafast laser (100 fs pulselength, KiF-laser, focal intensity $8\times10^{17}\,\mathrm{W\,cm^2}$) forms a plasma in an extended Xe-cluster gas plume as a function of the backing pressure. At higher backing pressures, the laser absorption is stronger in the first part of the cluster gas plume that shortens the length of the plasma and moves it out of the center of the plume. Because our laser and cluster gas parameters are not far from Miura's ones we set up a simple source model that is based qualitatively on the experimental findings of Miura. We regard only a one-dimensional plasma column in a 1.4 mm diameter cluster gas plume. From [14], an exponential decrease of the plasma source length versus backing pressure and a respective source movement is approximated. At very low-backing pressures, a centered position of the plasma column is given. In view of the laser propagation, the plasma start point is kept at a fixed position whereas the end point of the plasma column moves closer to the start with increasing density and cluster size. Our detection geometry is schematically depicted in the inset of Fig. 6. The signal of the plasma source is scaled linearly with the average atom density and the absorption [39] of the ambient cluster gas is calculated in dependence of the viewing angle of each source point. Because of inadequate knowledge of the EUV absorption in the ionized plasma, it is set to zero. In Fig. 6, we depict the registered emission at 13.4 nm versus backing pressure together with a function plot of our simple target model. Both curves are fitted together in dependence of one parameter for the signal height and one for the source extension. From Fig. 6, it is visible that the general behavior of signal increase and decrease can be reflected with the simple model, which of course cannot account for all the details of the experiment.

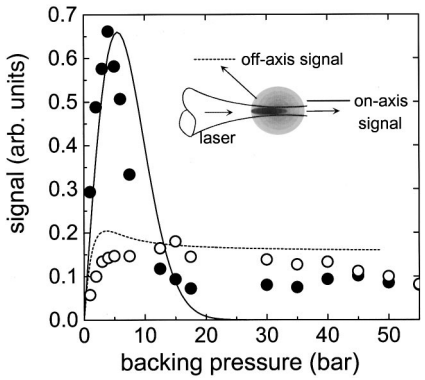

FIG. 6. Registered on-axis (closed square) and off-axis (open square) emission data at 13.4 nm in comparison to a computed signal (solid line–on axis, dotted line–off axis) on the basis of a simple geometric target model that is supported by the experimental findings of [14] (details, see text); inset shows detection geometry

V. EUV YIELD IN DEPENDENCE ON LASER POLARIZATION

Several experiments ([e.g., [4,8]) have revealed that collisional processes can play an important role for cluster heating resulting in the release of highly energetic ions up to MeV energies and hard x-ray emission. Therefore, it is of interest to what extent collisional heating of the electrons by inverse bremsstrahlung and stimulated Raman scattering [5] influence the ion species being responsible for the EUV emission looked at in this paper.

Before collisional heating of the laser plasma can occur, an initial ionization of the system has to take place. Optical-field ionization is the relevant process if high-intensity ($>10^{15}\,\mathrm{W/cm^2}$) ultrashort laser pulses are applied. For our focal intensity $\sim2\times10^{18}\,\mathrm{W/cm^2}$ it is obvious that ionization rates [40] from Xe to Xe XII are several orders of magnitude higher than an estimated maximum collisional ionization rate from Xe X to Xe XII that is in a range of 10^9–$10^{10}\,\mathrm{s^{-1}}$ [41]. Indeed, the laser intensity applied here is capable to produce ions up to Xe XXVI. Therefore, it is worthwhile to think about a change of the laser parameters in such a way that the laser field and the following tunneling process directly influence the spectrum of the initially ionized electrons. This can be done by changing the laser polarization from linear to circular [42]. The experiment may show whether this change is visible or ''washed out'' by following collisions.

From theoretical considerations, however, EUV spectra generated with linearly and elliptically polarized laser light should show a significant difference due to resulting higher energies of electrons field ionized with circularly polarized light [43–45]. Up to now, experiments have verified this mechanism in low-density gas targets [43,44], where other heating mechanisms are ineffective. Contrary to this, in case of high-density gas jets or in cluster targets the initial field ionization is thought to be followed by further collisional processes that in turn modify the ionic state distribution. Furthermore, defocusing arises from a refractive index gradient that is caused by an ionization variation across the beam [44] and that makes the picture more complicated. Because of these difficulties, no conclusions could be drawn how sensitive the polarization influences the ionization of a large Xe-cluster target and the related EUV yield. Therefore, we proceed with a polarization-dependent excitation experiment that was not reported so far for Xe clusters.

Circularly polarized laser light was produced by inserting a λ/4 plate in the beam. An obvious difference in the emission yield using the two different polarization states was detected with the off-axis spectrometer as depicted in Fig. 6. In the whole range of relevant Xe backing pressures, the emission around 13.4 nm is about two times higher if circularly instead of linearly polarized light is used. At 10 bar the ratio is about three times. The same feature was registered for the 10–15 nm emission band in off-axis direction.

In Fig. 8, emission data at 13.4, 11.4, and 7.5 nm from the on-axis spectrometer are collected. At 11.4 and 13.4 nm there is still some enhancement with the circular polarization visible, but it is only a factor between 1.1 and 1.2 at peak signal. Once more, similar to the discussion concerning Figs. 5 and 6, the peak signal level detected with the on-axis spectrometer is up to 2–3 times higher compared to the pressure optimized value for the off-axis one. From our experimental findings, we can thus conclude that the emission signature in the 10 to 15 nm wavelength region is not totally determined by collisional processes. The influence of the initial field ionization is visible and a change in laser polarization can be used for EUV-yield optimization. In off-axis emission direction, possible features may be also concealed by absorption in the plasma regarding the signals at 11 and 13.4 nm. (For simplicity, this has been excluded in the simple target model discussed above, but it may be a too crude assumption for explaining all the data.) At 7.5 nm, the absorption in the ambient gas is much weaker and the emission is observed up to maximum pressure in off-axis direction (on axis, the spectrometer cuts at 10 nm). The 7.5 nm signal in Fig. 8(c) shows no clear dependence from polarization. Here, the emission is already carried by higher Xe-ionization stages, which suffer probably a stronger influence by collisional processes, which ''washes out'' the initial ionization imprint. Collisional excitation of higher ionization stages becomes important after initial ionization due to high-energy electrons (the rate coefficients for collisional ionization becomes higher with increasing electron temperature [41]). Very recently, Kumarappan *et al.* [46] found that the K_α emission in the keV range from Ar clusters does not vary with the laser polarization, which would support the observed trend by us. We would not attribute the signal variation in Fig. 8(c) to simple data fluctuation covering a range of about 20%, but its origin remains unrevealed in this paper. With increasing pressure and growing cluster size, collisions favor the production of higher ionized states, and thus, the emission center of gravity can be shifted to a shorter wavelength. This effect could not be detected conclusively in our limited wavelength range of observation and possible indications may be covered by EUV absorption as discussed above.

VI. CONVERSION EFFICIENCIES AND COMPARISON TO OTHER LASER-DRIVEN Xe SOURCES

Within a 2.2% bandwidth centered at 13.4 nm, a wavelength band where Mo:Si multilayer mirrors with highest reflectivity (~70%) can be provided, the total integrated off-axis flux in relation to the incident laser energy (conversion efficiency) is shown in Fig. 7. Here, we extrapolated the emission in 2π sr solid angle using the observation angle of 0.05 msr of the off-axis spectrometer. Averaging the off-axis (Fig. 7) and on-axis (Fig. 8) data, we can infer a maximum laser light into EUV-emission conversion efficiency (CE) of

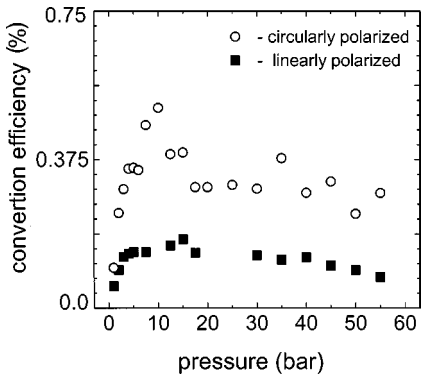

FIG. 7. Conversion efficiency at 13.4 nm related to recorded off-axis EUV emission and incident laser energy E_L at different Xe backing pressure when linearly ($E_L = 180$ mJ) and circularly ($E_L = 75$ mJ) polarized 800 nm laser light is used for excitation. Change in laser energy was due to operational reasons. In this range it does not change the conversion efficiency at constant polarization.

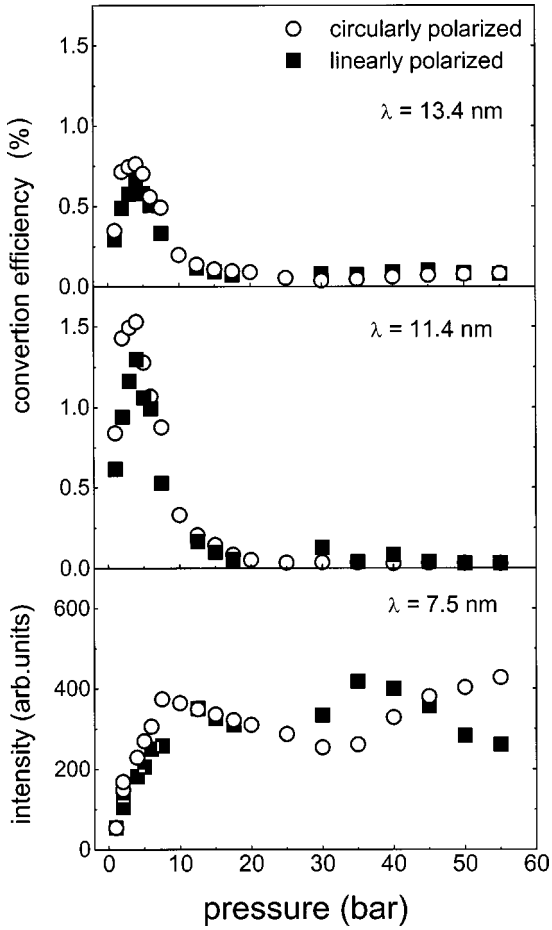

FIG. 8. Observed on-axis conversion efficiency for 13.4 nm, 11.4 nm, and relative intensity for 7.5 nm from Xe-cluster targets at different laser polarizations (cf. Fig. 6).

0.5% in 2π sr solid angle. At around 11.4 nm in respect to Mo:Be multilayer mirrors with highest reflectivity, the CE amounts to 2% in in 2π sr solid angle (cf. Fig. 5). Moreover, in the wavelength region from 10 to 15 nm, a CE up to 7.5% in 2π sr has been achieved. Our data exceed the conversion efficiencies obtained in experiments where Xe cluster targets were irradiated by KrF laser pulses with 100 fs pulse length [14]. Conversion efficiencies of 1.1% in 2π sr at 11 ± 0.27 nm and up to 7% in 2π sr in the region from 5 to 20 nm. have been reported. Some applications (e.g., lithography) require continuous or quasicontinuous-high-repetition rate-illumination where the single temporal pulse width does not and only the average power does matter. Therefore, it is important to compare with conversion efficiencies if other Xe aggregations (e.g., liquid) in a different laser interaction parameter regime (ns-laser pulses) are studied. Our CE at 13.4 nm is very similar to the related value given by Tichenor *et al.* [47] who has found for ns-irradiated Xe cluster/microdroplet-targets (cf. comment in [48]) a CE of about 0.7% in 2π sr and 2.2% bandwidth (BW). In contrast, for a Xe jet-target irradiated by YAG laser pulses of 10 ns duration CE's were reported [49] of 0.6% in 2π sr and 0.2% in 2π sr at 11.4 nm (1% BW) and 13.4 nm (2% BW), respectively.

VII. SUMMARY

Large Xe clusters (10^5–10^6 atoms per cluster) have been exposed with ultrashort (50 fs) and high intensity $(2-4)\times 10^{18}$ W/cm^2 pulses from a Ti:sapphire laser. Scaling and absolute yield measurements of EUV emission in a wavelength range between 7 and 15 nm in combination with cluster target characterization demonstrate the role of cluster size, average density, and target configuration for yield optimization. Maximum emission in the 11 to 13 nm emission band has been found with backing pressures between 5 and 15 bar. The registered anisotropy of on-axis and off-axis emission suggests an important influence of the source size, ion distribution, and radiation absorption within the ambient cluster gas. A simple model of a possible source geometry can explain main features of the observed signals. With the laser parameters used here $Xe^{9+},\ldots,Xe^{11+}$ ions are produced via optical-field ionization and are probably not essentially covered by further collisions. Therefore, the use of circularly polarized laser light results in the enhancement of the radiation signals in comparison to linearly polarized light. An absolute emission efficiency up to 0.5% in 2π sr at about 13.4 nm wavelength and 2.2% bandwidth shows the attractive application potential of this source. Based on available laser technology, further technical and application requirements can be chosen for a suitable Xe-target system for bright EUV radiation.

ACKNOWLEDGMENTS

A part of this paper was supported by BMBF-Project No. 13N7784. We thank A. Egbert (L. Z. H. Hannover) and C. Reinhardt (U. Hannover) for setting up partly the Rayleigh scattering experiments and the laser development team headed by M. Kalashnikov. Fruitful discussions with K. Janulewicz and H. Ruhl gave substantial impact to the interpretation of some EUV-emission results.

[1] *Emerging Lithography Technologies IV* (SPIE, Bellingham, WA, 2000), p. 3997.
[2] H. Kondo, T. Tomie, and H. Shimizu, Appl. Phys. Lett. **72**, 2668 (1998).
[3] *X-ray Microscopy and Spectromicroscopy*, edited by J. Thieme, G. Schmahl, D. Rudolph, and E. Umbach (Springer, Heidelberg, 1998).
[4] T. Ditmire, R. A. Smith, J. W. G. Tisch, and M. H. R. Hutchinson, Phys. Rev. Lett. **78**, 3121 (1997).
[5] T. Ditmire, T. Donnelly, A. M. Rubenchik, R. W. Falcone, and M. D. Perry, Phys. Rev. A **53**, 3379 (1996).
[6] A. McPherson, B. D. Thompson, A. B. Borisov, K. Boyer, and C. K. Rhodes, Nature (London) **370**, 631 (1994).
[7] T. Ditmire, J. W. G. Tisch, E. Springate, M. B. Mason, H. Hay, R. A. Smith, J. Marangos, and M. H. R. Hutchinson, Nature (London) **386**, 54 (1997).
[8] M. Lezius, S. Dobosz, D. Normand, and M. Schmidt, Phys. Rev. Lett. **80**, 261 (1998).
[9] K. Boyer, B. D. Thompson, A. McPherson, and C. K. Rhodes, J. Phys. B **27**, 4373 (1994).
[10] D. Stearns, R. Rosen, and S. Vernon, Appl. Opt. **32**, 6952 (1993).
[11] K. Skulina, C. Alford, R. Bionta, D. Makowieki, E. Gullikson, R. Soufli, J. Kortright, and J. Underwood, Appl. Opt. **34**, 3727 (1995).
[12] J. Underwood, in *Extreme Ultraviolet Lithography*, edited by G. Kubiak and D. Kania, Vol. 4 of *Trends in Optics and Photonics Series* (Optical Society of America, Washington, D. C., 1996), pp. 162–166; G. D. Kubiak, L. J. Bernardez, and Kevin Krenz, Proc. SPIE **3331**, 81 (2000).
[13] J. Murphy, D. White, A. MacDowell, and O. Wood II, Appl. Opt. **32**, 6920 (1993).
[14] E. Miura, H. Honda, K. Katsura, E. Takahashi, and K. Kondo, Appl. Phys. (N.Y.) **70**, 783 (2000).
[15] P. V. Nickles, M. Kalachnikov, P. J. Warwick, K. A. Janulewicz, W. Sandner, U. Jahnke, D. Hilscher, M. Schnürer, R. Nolte, and A. Rousse, Kvant Elektron. (Moscow) **27**, 165 (1999) [Quantum Electron. **29**, 444 (1999)].
[16] M. Dammasch (private communication).
[17] T. Wilhein, S. Rehbein, D. Hambach, M. Berglund, L. Rymell, and H. M. Hertz, Rev. Sci. Instrum. **70**, 1694 (1999).
[18] O. F. Hagena and W. Obert, J. Chem. Phys. **56**, 1793 (1972).
[19] O. F. Hagena, Surf. Sci. **106**, 101 (1981); O. F. Hagena, Rev. Sci. Instrum. **63**, 2374 (1992).
[20] J. Wormer, W. Guzielski, J. Stapelfeldt, and T. Moller, Chem. Phys. Lett. **159**, 321 (1989).
[21] A. J. Bell, J. M. Mestdagh, J. Berlande, X. Biquard, J. Cuvellier, A. Lallement, P. Meynadier, O. Sublemontier, and J.-P. Visticot, J. Phys. D **26**, 997 (1993).

[22] H. P. Birkhofer, H. Haberland, M. Winterer, and D. R. Worsnop, Ber. Bunsenges, Phys. Chem. **88**, 207 (1984).
[23] E. Springate, N. Hay, J. W. G. Tisch, M. B. Mason, T. Ditmire, M. H. R. Hutchinson, and J. P. Marangos, Phys. Rev. A **61**, 063201 (2000).
[24] A. J. Bell, J. M. Mestdagh, J. Berlande, X. Biquard, J. Cuvellier, A. Lallement, P. Meynadier, O. Sublemontier, and J-P. Visticot, J. Phys. D **26**, 994 (1993).
[25] M. Lewerenz, B. Schilling, and J. P. Toennies, Chem. Phys. Lett. **206**, 381 (1993).
[26] R. Karnbach, M. Joppien, J. Stapelfeldt, J. Wormer, and T. Moller, Rev. Sci. Instrum. **64**, 2838 (1993).
[27] T. Ditmire, R. A. Smith, R. S. Majoribanks, G. Kulcsar, and M. H. R. Hutchinson, Appl. Phys. Lett. **71**, 166 (1997).
[28] K. Kondo, A. B. Borisov, C. Jordan, A. McPherson, W. A. Schroeder, K. Boyer, and C. K. Rhodes, J. Phys. B **30**, 2707 (1997).
[29] J. Zweiback, T. Ditmire, and M. D. Perry, Phys. Rev. A **59**, R3166 (1999).
[30] J. Blackburn, P. K. Carroll, J. Costello, and G. O'Sullivan, J. Opt. Soc. Am. **73**, 1325 (1983).
[31] V. Kaufman, J. Sugar, J. L. Tech, J. Opt. Soc. Am. **73**, 691 (1983).
[32] G. O'Sullivan, J. Phys. B **15**, L765 (1982).
[33] M. McGeoch, Appl. Opt. **37**, 1651 (1998).
[34] H. Fiedorowicz, A. Bartnik, M. Szczurek, H. Daido, N. Sakaya, V. Kmetik, Y. Kato, M. Suzuki, M. Matsumura, J. Tajima, T. Nakayama, and Th. Wilhein, Opt. Commun. **163**, 103 (1999).
[35] M. A. Klosner and W. T. Silfast, J. Opt. Soc. Am. B **17**, 1279 (2000).
[36] H. Honda, E. Miura, K. Katsura, E. Takahashi, and K. Kondo, Phys. Rev. A **61**, 023201 (2000); B. A. M. Hansson, L. Rymell, M. Berglund, and H. M. Hertz, Microelectron. Eng. **53**, 667 (2000).
[37] Y. L. Shaö, T. Ditmire, J. W. G. Tisch, E. Springate, J. P. Marangos, and M. H. R. Hutchinson, Phys. Rev. Lett. **77**, 3343 (1996).
[38] O. F. Hagena, Surf. Sci. **106**, 101 (1981).
[39] http://www-cxro.lbl.gov
[40] N. H. Burnett, P. B. Corkum, J. Opt. Soc. Am. B **6**, 1195 (1989).
[41] W. Lotz, Z. Phys. **216**, 241 (1968).
[42] P. B. Corkum, N. H. Burnett, and F. Brunel, Phys. Rev. Lett. **62**, 1259 (1989).
[43] G. Pretzler and E. E. Fill Phys. Rev. E **56**, 2112 (1997).
[44] E. E. Fill, J. Opt. Soc. Am. B **11**, 2241 (1994).
[45] G. J. Pert, J. Phys. B **32**, 27 (1999).
[46] V. Kumarappan, M. Krishnamurthy, D. Mathur, and L. C. Tribedi, Phys. Rev. A **63**, 023203 (2001).
[47] D. A. Tichenor, G. D. Kubiak, W. C. Replogle, L. E. Klebanoff, J. B. Wronosky, L. C. Hale, H. N. Chapman, J. S. Taylor, J. A. Folta, C. Montcalm, R. M. Hudyma, K. A. Goldberg, and P. Naulleau, Proc. SPIE **3997**, 48 (2000).
[48] E. Parra, I. Alexeev, J. Fan, K. Y. Kim, S. J. McNaught, and H. M. Milchberg, Phys. Rev. E **62**, R5931 (2000).
[49] B. A. M. Hansson, M. Berglund, O. Hembers, and H. M. Hertz, Proc. SPIE **3997**, 729 (2000).